CrossMark

Dielectric properties of bismuth niobate films using LaNiO$_3$ bottom electrode

L. F. Goncalves[1] · L. S. R. Rocha[1] · C. C. Silva[1] · J. A. Cortés[1] · M. A. Ramirez[1] ·
A. Z. Simões[1]

Abstract Bi$_3$NbO$_7$ (BNO) thin films were deposited on Pt/TiO$_2$/SiO$_2$/Si (100) and LaNiO$_3$ bottom electrode substrates at room temperature from the polymeric precursor method. X-ray powder diffraction was used to investigate the formation characteristics and stability range of the tetragonal modification of a fluorite-type solid solution. The results showed that this tetragonal, commensurately modulated phase forms through the intermediate formation of the incommensurately modulated cubic fluorite phase followed by the incommensurate-commensurate transformation. LaNiO$_3$ (LNO) bottom electrode strongly promotes the formation of high intensity (111) texture of BNO films. The dielectric constants of the films increased from 192 to 357 at 1 MHz with the bottom electrode while the leakage current behavior at room temperature of the films decreased from 10^{-7} to 10^{-8} A/cm^2 at a voltage of 5 V. The reduction of dc leakage current is explained on the basis of relative phase stability and improved microstructure of the material. The capacitance density of 75 fC/μm^2, dielectric loss of 0.04 % at 1 MHz, and breakdown strength of about 0.30 MV/cm is compatible with embedded decoupling capacitors applications.

✉ L. S. R. Rocha
drleandrosrr@gmail.com

[1] Univ. Estadual Paulista- Unesp – Faculdade de Engenharia de Guaratinguetá, Av. Dr Ariberto Pereira da Cunha 333, Portal das Colinas, P.O. Box 355, Guaratinguetá, São Paulo 12.516-410, Brazil

1 Introduction

Investigations on dielectric thin films have increased for the application to embedded decoupling capacitors (EDCs) for printed circuit boards [1, 2]. The radio frequency (RF) or analog/mixed metal–insulator–metal (MIM) capacitors in semiconductor devices also require a dielectric thin film with a low processing temperature because of the limitation of the very large scale integration back-end line temperature (<400 °C). These capacitors need high capacitance density that can be obtained by using a dielectric film with a high dielectric constant (k) or by decreasing the film thickness. However, decreasing the film thickness induces a high leakage current with a low breakdown voltage. Therefore, it is important to develop a very thin dielectric film with a low processing temperature and a low leakage current density for application to embedded and RF MIM capacitors.

The utilization of EDCs can be a powerful solution for minimizing equivalent series inductance (ESL) of power delivery circuits or packages. To fabricate a capacitor-embedded printed circuit board (PCB) for in-line processing, it is essential to obtain dielectric materials with high permittivity and low dielectric loss when processed with low cost precursors. To achieve these characteristics, studies on bismuth-based dielectrics with a high dielectric constant and a small dielectric loss were made by many research groups [3–12]. BNO has a cubic fluorite structure in nature and is known to have high dielectric constants (100) with low dielectric loss tangent (10×10^{-4}) with an applied frequency of 1 MHz [4]. At room temperature, bismuth niobate Bi$_3$NbO$_7$ can exhibit two crystallographically modulated modifications, which are both derived from the high-temperature "delta" form of bismuth oxide, δ-Bi$_2$O$_3$. Indeed, for temperatures between 1003 and

1098 K, δ-Bi_2O_3 belongs to an oxygen deficient fluorite structure (25 % of unoccupied oxygen sites), being one of the best solid-state ionic conductors known so far. In fact, the cubic incommensurate (also called type-II) and the tetragonal-commensurate structures (type-III) are interesting because of their high ionic conductivities, allowing it to be applied in solid oxide fuel cells. The tetragonal commensurate form exhibits encouraging dielectric properties, which are combined with good sinterability, and as a result, it is a candidate for being a high-permittivity glass free layer in the developing of low-temperature cofired ceramic technology for microwave (MW) devices [13].

Several attempts have been made to enhance the crystallization ability of thin films and metallic oxide electrodes [14]. The use of a domestic microwave furnace as a way to process materials has opened an opportunity to enhance crystallization with a lower annealing processing time since it decreases the interfacial reactions between ferroelectric thin films and electrodes also improving control over the crystallographic orientation of the thin films [15]. The purposes of this study are to use $LaNiO_3$ as the metal oxide bottom electrode and, at the same time, to provide a template to grow better quality BNO films with preferred orientation. Our results demonstrate promising properties better than those of other reports. It is well known that perovskite oxide electrode, such as $SrRuO_3$, $LaNiO_3$, and $BaPbO_3$, effectively improved crystal growth and electric properties of oxides [16, 17]. Of particular interest, the LNO electrode is promising to induce the preferred-orientation and improve the film/electrode interface of dielectric films. In previous work, the 200 nm thick BNO films deposited on platinum coated silicon substrates exhibit a dielectric constant of 170, capacitance density of 200 nF/cm^2, dielectric loss of 0.4 % at 1 MHz, and a leakage current density of approximately 1×10^{-7} A/cm^2 at 5 V. They show breakdown strength of about 0.25 MV/cm [18]. To our knowledge, no report is available on the dielectric characteristics of BNO films on the oxide electrode. Therefore, we investigated the role exerted by the bottom electrode on dielectric reliability of BNO films crystallized by the polymeric precursor method as a new candidate for dielectric capacitors processed at PCB-compatible temperatures. This demonstration of low-cost process, high-performance, and thin-film capacitors is surely an important step toward the development of EDCs.

2 Experimental procedure

BNO and LNO thin films were prepared by the polymeric precursor method, as described elsewhere [14]. The films were spin coated on $Pt/Ti/SiO_2/Si$ substrates by a commercial spinner operating at 5000 revolutions/min for 30 s (spin coater KW-4B, Chemat Technology). An excess of 5 % wt of Bi was added to the solution aiming to minimize the bismuth loss during the thermal treatment. Each annealing cycle of the thin film was performed at 700, 800 and to 860 °C for 2 h in the conventional furnace under static air atmosphere. The film thickness was reached by repeating 10 times the spin-coating and heating treatment cycles. Each layer of the LNO bottom electrode thin films was pre-fired at 400 °C for 2 h in a conventional oven and crystallized at 700 °C for 10 min in the microwave furnace. Through this process, we have obtained thickness values of about 100 nm (5 layers) for the bottom electrodes and around 200 nm for BNO (10 layers) on Pt coated silicon substrates and 280 nm for $LaNiO_3$ coated Pt substrates, reached by repeating the spin-coating and heating treatment cycles. The thickness of the annealed films was measured using scanning electron microscopy (Topcom SM-300) at the transversal section. In this case back scattering electrons were used. Phase analysis of the films was performed at room temperature by X-ray diffraction (XRD) using a Bragg–Brentano diffractometer (Rigaku 2000) and CuKα radiation in the 2θ range from 20 to 60° with 0.03°/min^{-1}. The morphology of the films was observed using a high resolution field-emission gun scanning electron microscopy FEG-SEM (Supra 35-VP, Carl Zeiss, Germany). Top Au electrodes (300 μm) were prepared by sputtering through a shadow mask at room temperature acquiring a metal–semiconductor–metal (MSM) capacitor configuration for the electrical and dielectric measurements. The current–voltage characteristic was measured at (*Keithley 6430*) with a 10 μA current compliance (used here to prevent the permanent damage on the films). The relative dielectric permittivity (ϵ_r) and the dissipation factor (tan δ) were obtained by impedance spectroscopy measurements in the frequency range from 100 Hz to 2 MHz by employing a frequency response analyzer (HP, Model 4192A). All measurements were performed at room temperature.

3 Results and discussion

Figure 1a, b presents the XRD patterns of BNO films deposited on platinum coated silicon and LNO substrates. The films were well crystallized at the processing temperature under investigation. As can be seen, a fluorite-type structure is obtained. No traces of $Bi_5Nb_3O_{15}$ [19] and δ-Bi_2O_3 phase (*a* 55.648 Å [20]) appears to be present. The Bi_3NbO_7 phase belongs to the classical fluorite-type structure and the main peak is located at $2\theta = 28°$. The additional, i.e., satellite, reflections of low intensity related to (2 0 0), (2 2 0), (3 1 1) planes indicate a superlattice ordering, known to occur in this systems. The satellite
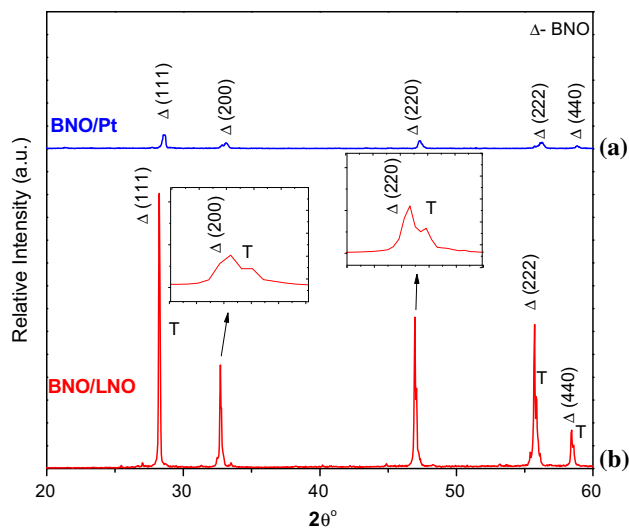
Fig. 1 X-ray diffraction of BNO thin film deposited by the polymeric precursor method and annealed from 700 to 860 °C in static air for 2 h at: (*a*) Pt and (*b*) LNO coated Pt substrates. *Inset* of Fig. 1 showing the tetragonal splitting

reflections are present at the same positions as those reported in the literature, and confirm the similar incommensurate modulation of Type II, as described by Miida et al. [21]. The most intense diffraction peaks appear at the same 2θ angles, but due the temperature employed to crystallize the film at 860 °C a very noticeable tetragonal splitting is observed, which can be seen as insets indicated by the arrows. A model proposed by Ling and Johnson [22] attempt to fit data from neutron diffraction patterns for the Type III modulation structure related to these compounds and further studies could possibly be done to reinforce the phase transition. The XRD patterns can be identified and indexed using the standard XRD data of Bi_3NbO_7 (JCPDS 86-0875), with space group Fm3 m. The six peaks in the patterns were indexed to (3 1 1) (1 1 1), (2 0 0), (4 0 0), (2 2 0), (2 2 2) and (4 4 0) planes respectively, and can match well with the standard peaks of Bi_3NbO_7. The X-ray pattern for the LNO coated Pt substrates (Fig. 1b) showed highly crystalline (111) Bragg peak. The LNO layer not only serves as a useful metal oxide bottom electrode, but also forms a template which enables growth of high quality BNO films (Fig. 1b). As seen in XRD peaks of BNO thin films, the layered perovskite (111) peak was found. This means that the BNO thin film consisted of a single-phase with a transition from cubic to tetragonal phase which is a certain kind of disorder–order or incommensurate–commensurate phase transition. This is an interesting result considering that the lattice mismatch between LNO ($a = 0.384$ nm) and BNO ($a = 0.54788$ nm) is quite larger. It is emphasized that the use of $LaNiO_3$ film (even with big lattice mismatch with Bi_3NbO_7) on the same Pt and the

complex cycling firing steps at the maximum 860 °C lead to better dielectric permittivity and phase transformation from cubic to tetragonal, see inset in Fig. 1. The use of microwave furnace, with the SiC-susceptor placed below the films, suggests that the crystallization of the bottom electrode starts from the film-substrate interface leading to a high crystalline oxide. Therefore, the versatility of the microwave treatment in the control of the film structure is desirable since the time required to obtain the phase is reduced with proper understanding and control, many technically important materials can be heated rapidly, uniformly, selectively, less expansively and with greater control than is possible with conventional methods. As a consequence, the deposition of BNO phase on the LNO bottom electrode leads to high crystallization along (111) direction since it plays an important role as nucleation sites for the formation of BNO thin films. The positive role of LNO may be caused by the decrease in the nucleation activation energy that allows us to obtain a good crystallization at this temperature. In order to understand the possible coordination of both niobium and bismuth atoms in Bi_3NbO_7, we propose different models of possible rearrangement of the oxygen–fluorite-type network. From the classical organization of M_4O_8-type fluorite, the displacement of some oxygen atoms keeps the overall M_4O_8 composition but changes some metallic coordination from CN = 8 to CN = 7 and CN = 6. Pursuing this line, some oxygen can be removed (oxygen loss), creating vacancies and leading to a nonstoichiometric fluorite-type network, i.e., M_4O_7 composition. Such hypothesis implies local anionic reorganization in the 3-dimensional network in order to give a classical oxygen octahedron around the niobium atoms, with bismuth atoms accepting a wide variety of oxygen polyhedra more or less distorted by the stereochemical influence of its lone pair. Such an arrangement can occur in all directions, giving rise to local differences of composition and order in the crystal. The experiments showed that the tetragonal phase with the $3 \times 3 \times 7$ superstructure appears at the temperature employed. Firing at 860 °C for 2 h, for instance, yields a sample in which both cubic and tetragonal phases were detected. From experiments performed to determine the thermal stability of the tetragonal Bi_3NbO_7 we noticed that during the film growth the cubic phase is formed first, and then if the right annealing conditions are used it transforms into the tetragonal phase. A periodicity in the tetragonal phase that is a rational multiple of the unit cell of the underlying fluorite structure indicates that the tetragonal phase, in contrast to the cubic phase, exhibits a commensurate superstructure ordering. This means that the transition from cubic to tetragonal phase in the case of Bi_3NbO_7 is a certain kind of disorder–order or incommensurate–commensurate phase transition. Such a phase transition

exhibits kinetics that is temperature dependent. Therefore, at higher temperatures, closer to the upper temperature limit (860 °C) of its thermodynamic stability, the formation of the tetragonal (ordered) phase is much more rapid than at the lower temperatures (700 °C).

Figure 2a, b shows AFM images of BNO thin films on the Pt coated Si with and without the LNO buffer layer. The thin films on the Pt coated Si had a relatively rough surface. The mean roughness of the surface (RMS) was 6.4 nm with a grain size of 85 nm. The rough surface may be due to the presence of plate-like perovskite grains. The thin films on the LNO buffer layer had a homogeneous and dense microstructure. The RMS value was decreased to as low as 3.2 nm, besides rising of grain size to 100 nm. AFM images also revealed that the surface of the BNO film with no buffer layer (Fig. 2a) exhibits plate-like grains while the surface of the film with buffer layer possesses rounded grains (Fig. 2b). The films crystallized on platinum substrates are random oriented and present less energetic favorable form (elongated grains) with a typical bismuth compounds. Meanwhile, the film crystallized on the LNO bottom electrode is strong textured and the grains tend to assume the more energetic favorable form (rounded).

Considering that the dielectric permittivity depends on several factors such as annealing temperature, grain size, type of electrodes and phase composition it could be observed an increase in dielectric permittivity with the modification in the grains shape.

To confirm the surface morphology, FEG-SEM was carried out. The results are shown in Fig. 3. The BNO films crystallized on both platinum and LNO substrates are homogeneous, uniform and crack free indicating that the polymeric precursor method allows the preparation of films with controlled morphology. BNO film exhibit a homogenous structure being the deposition of the thin films performed by a nucleation and growth process at the surface of the substrates. Because the annealing conditions employed, the diffusion of species and the nucleation and growth rate increased affecting the grain size and shape of grains. Bismuth-based dielectric materials contain a bismuth metal in the as-deposited films which also may play an important
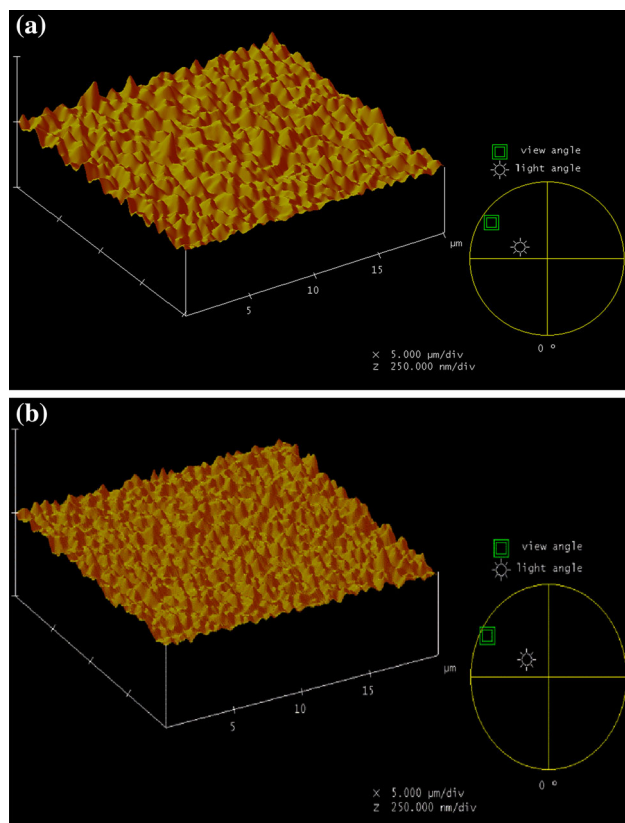

Fig. 2 AFM micrographies of BNO thin film deposited by the polymeric precursor method and annealed from 700 to 860 °C in static air for 2 h: **a** Pt and **b** LNO coated Pt substrates
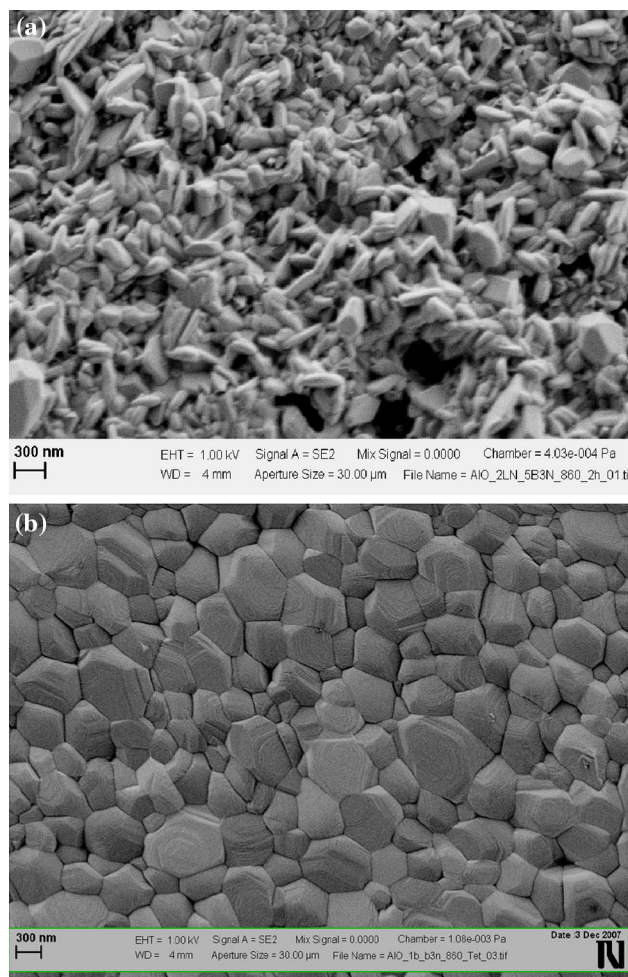

Fig. 3 FEG-SEM images of BNO thin film deposited by the polymeric precursor method and annealed from 700 to 860 °C in static air for 2 h: **a** Pt and **b** LNO coated Pt substrates

role in the formation of smooth and dense morphologies. A strongly marked difference in the film morphology can be observed for the different bottom electrodes. The films obtained on Pt coated substrates present a typical bismuth layer perovskite structure while the ones obtained on oxide electrode showed spherical grains. For films deposited on LNO, charge carriers (oxygen vacancies) trapped near the film-electrode interface, are minimized. These charges may be originated during the heat treatment process due to the decomposition of the polymeric precursor. It can be assumed that if oxygen vacancy accumulation near the film-electrode interface occurs during heat treatment, the conductive oxide can consume the oxygen vacancies by changing their oxygen nonstoichiometry and thus, the accumulation of oxygen vacancies near the interface is prevented or reduced affecting the shape and size of grains. The main reason causing the surfaces of the BNO films deposited on Pt and for the LNO coated Pt substrates can be originated from the difference in nuclear generation density between the Pt and the LNO electrode. After formation of the BNO film, the buffer layer disappears indicating that this conductive oxide acts not as barrier layer but as an initial nucleation of the BNO thin film with a very noticeable phase transition from cubic to tetragonal.

Dielectric properties of BNO thin films on the Pt coated Si with and without the LNO bottom electrode are presented in Fig. 4a, b. Because Bi_3NbO_7 shows an oxygen-deficient fluorite structure with a disordered long-range vacancy, good oxide ion conduction is expected. For other mixed oxides derived from δ -Bi_2O_3, a conductivity dominated by movement of oxygen vacancies has been reported [22]. The dielectric permittivity and loss factor at 1 MHz of the Pt/BNO/Pt capacitor were 192 and 0.4 %, respectively. The permittivity and dielectric losses of thin films decreased appreciably with frequency increasing. Similar dependency of permittivity and dielectric losses on frequency has been reported on Bi-contained pyrochlore ceramics [23]. The dielectric permittivity (ε) and loss factor (tan δ) of the Pt/LNO/Pt capacitor were 357 and 0.03 %, respectively, at 1 MHz and were almost independent of frequency. Little dependence of dissipation factor with frequency can be addressed to the presence of a barrier layer between the insulating film and the electrode surface or leaky grain boundaries. The larger dielectric permittivity can be correlated with the increased grain size, which was shown in the AFM micrograph. One can say that the LNO bottom electrode deeply influenciate the dielectric values of bismuth niobate thin films. The BNO thin film demonstrated very low dielectric loss values in the measurement frequency range. The dielectric losses were lower than 0.4 % in this temperature range. The dielectric behavior might be associated with the interfacial leakage conduction loss between grains. It was supposed that high
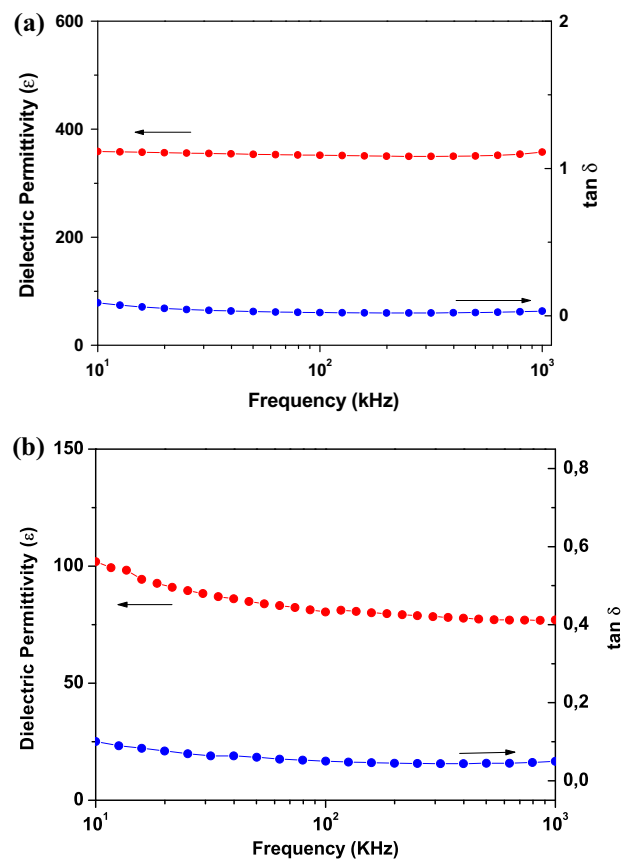

Fig. 4 Dielectric properties in dependence of frequency for BNO thin films annealed from 700 to 860 °C in static air for 2 h: **a** Pt and **b** LNO coated Pt substrates

density of interfacial defects in thin films with large porosity would enhance leakage conduction loss at interfaces between grains. The measured properties show that the presence of the observed grain boundary inclusions did not negatively affect the dielectric permittivity, which is close to that of bulk ceramics. The enhanced ε may stem from the crystallinity relating to the residual stress in the thin film. This enhancement may be due to the improvement between the BNO thin film and the electrode interface, which could be a result of the formation of a well developed structure as well as to the large grain size of the BNO thin films. This supports our idea that microwave oven treatments in the formation of the bottom electrode suppress the formation of a very low dielectric constant layer at the thin film/electrode interface, which is the main cause of the lower value of the dielectric permittivity related to many dielectric thin films. Regarding dielectric loss, the measurements suggest that low frequency loss values are significantly higher in a film annealed at Pt substrate which can be explained by the higher space charge concentration which again arises due to a higher oxygen vacancy concentration. Also, it can be noted that

dielectric properties (both the dielectric permittivity and the dielectric loss) improve appreciably which again emphasizes the superior quality of BNO deposited on LNO sintered films. It is possible that this decrease in the permittivity for the film deposited on Pt is caused by space charge polarization which is inherently related to the non-uniform charge accumulation. Due to the changes in the grain microstructure, the introduction of oxide electrode causes a more sensitive distortion of the perovskite lattice which leads to a reduction in the oxygen octahedron interstices. The distortion of the perovskite lattice can strengthen the structure fluctuation of BNO which can be account for different dielectric permittivity behavior. Since XRD data reveals structural identity on the level of the prototype cell and on the level of the superstructure modulation it is evident that the incommensurate-cubic phase undergoes a certain kind of disorder–order phase transition at 860 °C to the commensurate-tetragonal phase.

In potential electronic device applications of dielectric thin films it is desirable to understand the behavior of the dc-leakage current with the bias field. The mechanism of leakage current density is more difficult to establish in comparison to other physical properties materials. A large number of researchers have attempted to understand the leakage current characteristics of oxide ferroelectric thin films and low leakage current density is an important consideration for memory device applications [24, 25]. A typical leakage current characteristic for BNO thin film is given in Fig. 5. The curve was recorded with a voltage step width of 0.1 V and elapsed time of 1.0 s for each voltage; here the measured logarithmic current density (log J) versus the voltage (V) is shown. It can be seen that there are two clearly different regions. The current density increases

linearly with the external electric field in the region of low electric field strengths, suggesting an Ohmic conduction. This ohmic behavior occurs in insulating film as long as the film is quasi-neutral, that is, as long as the bulk generated current in the film exceeds the current due to injected free carriers from the electrode. This current would be due to the hopping conduction mechanism in a low electric field, because thermal excitation of trapped electrons from one trap site to another dominates the transport in the films. At higher field strengths the current density increases exponentially, which implies that at least one part of the conductivity results from Schottky or Poole–Frenkel emission mechanism. The leakage current density at 5.0 V is equal to 10^{-7} A/cm^2 with a breakdown strength of 0.25 MV/cm for the BNO deposited on Pt coated silicon substrates and 10^{-8} A/cm^2 with a breakdown strength of 0.30 MV/cm for the BNO on LNO coated Pt substrates. For the leakage current comparison, the total film thickness is assumed. The measured leakage is attributed to LaNiO$_3$ electrode. No other capacitive layer was evidenced with supporting experimental data. Since different top and bottom electrodes were used we assume that the bulk controls the properties of such film revealing a symmetric I–V characteristic for both voltage polarities. Therefore, the low leakage current can be an effect of the grain size, which implies several grain boundaries along the current flow acting as potential barriers. The leakage current density of the BNO film was slightly reduced by the insertion of the bottom electrode. This indicates that the role of oxide is to decrease the nucleation probability, to favor the growth of textured films, besides to consume the oxygen vacancies by changing their oxygen nonstoichiometry. Thus, the buffer layer does not prevent a possible small accumulation of oxygen vacancies near the interface. It does, however, provide films with larger grain sizes due to a reduced nucleation rate. At low fields the leakage current density increases linearly with the applied field according to an Ohmic characteristic. At higher fields, these films exhibit nonlinear J–V relationships. Comparing with literature data, our films present a higher leakage current than the films obtained on highly oriented LNO-buffered Pt/Ti/SiO$_2$/Si substrates by sol–gel process (1×10^{-7} A/cm^2) [26, 27]. Since the conductivity is strongly affected by the characteristics of the film-electrode interface, the lower leakage current observed in the literature may be probably attributed to differences in grain size, density, and preferred orientation due to differences in the metal–ferroelectric–metal configuration. Our results indicate that there is a strong change in leakage current density with the bottom electrode. The leakage current density for the films deposited on LNO electrode is lower when compared to the films deposited on Pt electrode. Such a reduction in leakage current density may be attributed to high oxygen affinity of
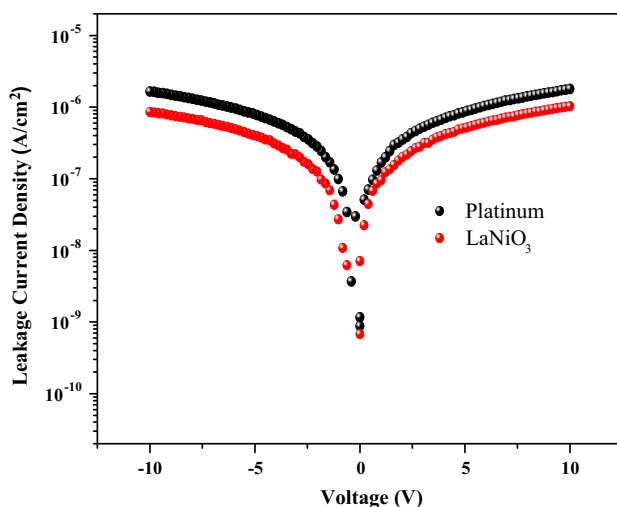

Fig. 5 Typical *I–V* curve of BNO thin films annealed from 700 to 860 °C in static air for 2 h: **a** Pt and **b** LNO coated Pt substrates

these electrodes avoiding that oxygen in the electrode material to be depleted by the ferroelectric material, thus leaving an oxygen deficient layer of the electrode at the interface and increasing the contact resistance. This avoids the migration of charge species to the electrode-film interface and can be related to the grain morphology. From these results it can be suggested that the morphology of ferroelectric films play an important role in their conductivity properties [28, 29].

Figure 6 shows the bias-field dependence of the capacitance at a measurement frequency of 1 MHz for BNO film on platinum coated silicon and LNO bottom electrode. Although positive and negative biases were employed there is no evidence of hysteresis behavior, confirming the absence of domain structure. The dielectric permittivities calculated from C–V curves are around 192 and 357 agreeing with the dielectric permittivity as a function of frequency. The tunability is defined as $(C_0 - C_v)/C_0$ where C_0 and C_v are the capacitance values at zero and maximum DC-voltage levels. For a field of 1 MV/cm and a measurement frequency of 1 MHz, maximum tunability of 28 and 44 % was obtained. The tunability showed no hysteresis. Studies are underway to clarify the role of film strain due to the differences in thermal mismatch and its dependence on tunability. In view of the XRD measurements discussed above, it was suggestive that the higher tunability of such film could be a result of a commensurate superstructure ordering, as well as the relatively larger grain size, since the larger grain size could be a positive factor to dielectric tunability.

The charge storage density were estimated from the C–V characteristics using the relationship $Q_c = \varepsilon_0 \varepsilon_r E$, where ε_0 is the permittivity of free space, ε_r is the relative permittivity and E is the applied field (Fig. 7). A practical DRAM capacitor requires a low leakage current density (LCD) $< 10^{-8}$ A/cm^2 and a charge storage density of about 35 fC/μm^2 [30]. From Fig. 7 it may be seen that this would be satisfied already at E = 0.27 MV/cm for Pt/BNO/Pt and 0.10 MV/cm for Pt/LNO/Pt.

Figure 8a, c show the Bode complex impedance diagram for the BNO film. The feature at the highest measuring frequency is characteristic of R–L resonance form, the measuring leads and electrode itself. On the other hand, the region of lower frequencies shows an inverse behavior. This range accounts for grain–grain junctions and controls the global conductivity response, being strongly related to the dielectric mechanism. Moreover, the complex capacitive diagram indicates that the capacitance of the electrodes is hardly affected by the structure of the ferroelectric material. Figure 8b, d show the Bode capacitive diagrams, confirming the effects of the interface on the capacitance from intermediate to low frequencies. Such a relaxation pattern can be described by an equivalent circuit consistent with three parallel contributions: the "high frequency" limit related to grain boundary capacitances, the complex incremental capacitance at intermediate frequencies related to the relaxation of the particular structure found in the space charge region, and finally, in the low frequency region, the term representing the dc conductance of the multi-junction device. The high frequency region of the complex capacitance diagrams shows the presence of a dipolar relaxation process possessing a near-Debye pattern (see Bode capacitive diagrams of Fig. 8). It is important to emphasize here that, in the present discussion, because the dielectric properties may be strongly related to the a multi-junction domain, [29, 31], it is inappropriate to use parameters such as dielectric permittivity or susceptibility, since it is almost impossible to know enough about the
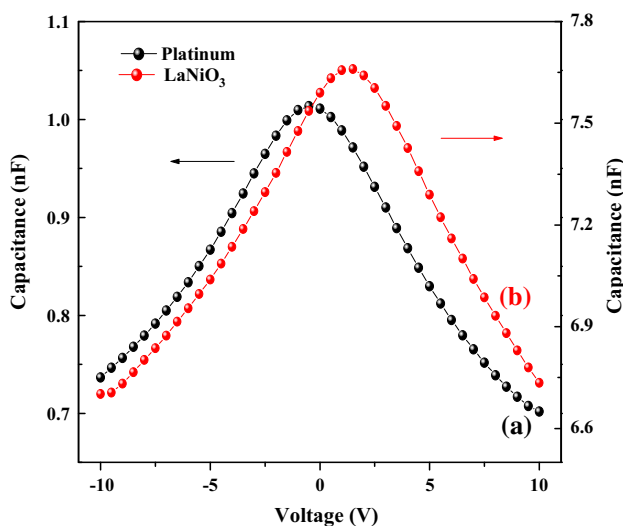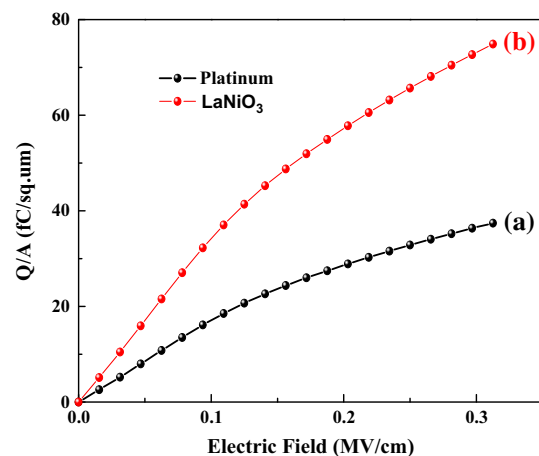

Fig. 6 Capacitance voltage characteristic for BNO thin films annealed from 700 to 860 °C in static air for 2 h: (a) Pt and (b) LNO coated Pt substrates

Fig. 7 Charge storage density for BNO thin films annealed from 700 to 860 °C in static air for 2 h: (a) Pt and (b) LNO coated Pt substrates
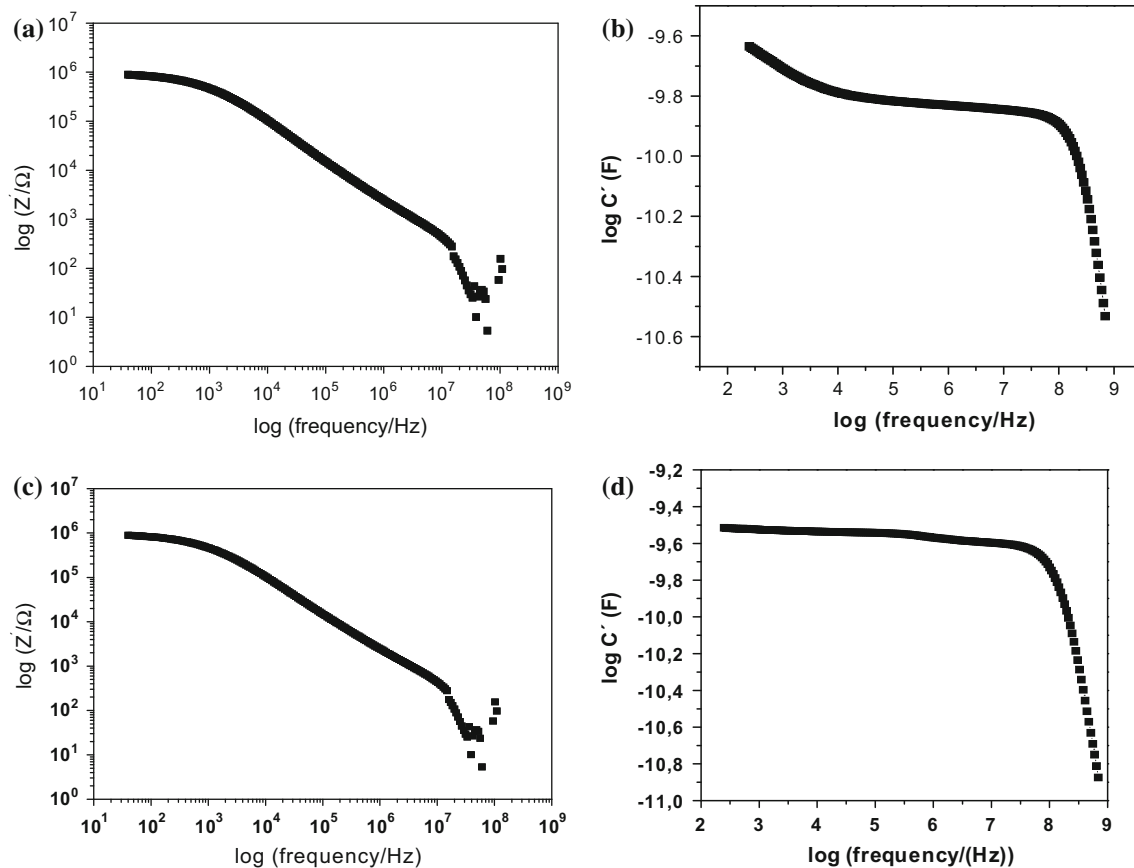
Fig. 8 Bode capacitive diagrams for the BNO films. Logarithm of real part of the complex capacitance as a function of frequency. **a**, **c** Pt and **b**, **d** LNO coated Pt substrates

geometry, i.e., the thickness of the region in question (domain boundaries existing in the grain), to determine the complex permittivity. That is why we prefer to express the response in terms of complex capacitance (C*) instead of complex dielectric form (ε*) [32]. Responses due the sample-electrode interfaces which have very high polarization both due the thin film geometry of the interface and the high charge density due to any space charge effects are evident and appear at the lowest measuring frequencies. For practical applications, the films are preferred to be less conductive. As previously verified in early work of our group [33], the oxygen vacancies concentration is affected by the annealing atmosphere. The thermal treatment in oxidant atmosphere in materials with *p*-type conductivity increases defects as Bi or Ti vacancies. This results in an increase in conductivity with increasing oxygen content indicating that the mobile carriers are positively charged and that the possibility of hopping through the Bi ion can be considered. Taking into account that we have annealed the BNO films in static air, the oxygen vacancies are ordered, avoiding oxygen ions to migrate and therefore reducing conductivity. Thus, less conditions for the trapping of electrons results in a highly resistance film.

4 Conclusions

LaNiO$_3$ bottom electrode was found to be effective buffer layer for improvement crystal structure and electrical properties of BNO thin films. The film crystallized on oxide electrode was a single phase and showed random orientation. The dielectric properties of BNO thin films were strongly affected by the bottom electrode and surface grain size. The LNO bottom electrode produced a BNO film with a dielectric loss lower than 0.03 % and the maximum voltage tunability of 44 % with an applied bias field of 0.25 MV/cm under 1 MHz were obtained by the chemical solution deposition. The very low losses and electric field tunable dielectric constant may make these films promising for tunable capacitor applications. The films show relatively large high dielectric constant, which originates from textured orientation. These excellent dielectric and structural properties are favored by the LNO buffer layer, which reduces the initial nucleation rate when crystallizing the BNO thin film. The low conductivity of the BNO thin film on LNO buffer layer is a consequence of oxygen vacancies ordering, avoiding oxygen ions to migrate and less conditions for the trapping of electrons.

Finally, we would like to propose LNO as a promising bottom electrode for the deposition of high intensity textured bismuth niobate thin films.

References

1. J.H. Park, W.S. Lee, N.J. Seong, S.G. Yoon, S.H. Son, H.M. Chung, J.S. Moon, H.J. Jin, S.E. Lee, J.W. Lee, H.D. Kang, Y.K. Chung, Y.S. Oh, Bismuth–zinc–niobate embedded capacitors grown at room temperature for printed circuit board applications. Appl. Phys. Lett. **88**(19), 192902 (2006)

2. J.H. Park, S.G. Yoon, H.D. Kang, J.W. Lee, W.C. Kim, S.T. Lim, S.H. Sohn, J.S. Moon, H.J. Jin, H.M. Jung, S.E. Lee, Y.K. Chung, Structural and dielectric properties of cubic fluorite Bi_3NbO_7 thin films as-deposited at 298 K by PLD for embedded capacitor applications. J. Electrochem. Soc. **153**(10), F225–F227 (2006)

3. A.A. Maradudin, D.L. Mills, Scattering and absorption of electromagnetic radiation by a semi-infinite medium in the presence of surface roughness. Phys. Rev. B. **11**(4), 1392–1415 (1975)

4. R.L. Moreira, F.M. Matinaga, U. Pirnat, D. Suvorov, A. Dias, Optical phonon characteristics of incommensurate and commensurate modulated phases of Bi_3NbO_7 ceramics. J. Appl. Phys. **103**(9), 094108-1–095108-7 (2008)

5. S.N. Ng, Y.P. Tan, Y.H. Taufiq-Yap, Mechanochemical synthesis and characterization of bismuth–niobium oxide ion conductors. J. Phys. Sci. **20**(1), 75–86 (2009)

6. B.H. Park, S.J. Hyun, S.D. Bu, T.W. Noh, J. Lee, H.D. Kim, T.H. Kim, W. Jo, Differences in nature of defects between $SrBi_2Ta_2O_9$ and $Bi_4Ti_3O_{12}$. Appl. Phys. Lett. **74**(13), 1907–1909 (1999)

7. X.P. Wang, Z.J. Cheng, Q.F. Fang, Phase transition kinetics in Bi_3NbO_7 evaluated by in situ isothermal conductivity measurements. Chin. Phys. Lett. **24**(4), 1013–1016 (2007)

8. D. Zhou, H. Wang, X. Yao, L. Pang, Sintering behavior and microwave dielectric properties of $Bi_3(Nb_{1-x}Ta_x)O_7$ solid solutions. Mater. Chem. Phys. **110**(2–3), 212–215 (2008)

9. D. Zhou, H. Wang, X. Yao, Sintering behavior and dielectric properties of Bi_3NbO_7 ceramics prepared by mixed oxides and high-energy ball-milling method. J. Am. Ceram. Soc. **90**(1), 327–329 (2007)

10. H.C. Ling, M.F. Yan, W.W. Rhodes, High dielectric constant and small temperature coefficient bismuth based dielectric compositions. J. Mater. Res. **5**(8), 1752–1762 (1990)

11. H. Kagata, T. Inoue, J. Kato, I. Kameyama, Low-fire bismuth-based dielectric ceramics for microwave use. Jpn. J. Appl. Phys. **31**(9S), 3152–3155 (1992)

12. A. Mergen, W.E. Lee, Crystal chemistry, thermal expansion and dielectric properties of $(Bi_{1.5}Zn_{0.5})(Sb_{1.5}Zn_{0.5})O_7$ pyrochlore. Mater. Res. Bull. **32**(2), 175–189 (1997)

13. H. Wang, X. Yao, Structure and dielectric properties of pyrochlore–fluorite biphase ceramics in the Bi_2O_3–ZnO–Nb_2O_5 system. J. Mater. Res. **16**(1), 83–87 (2001)

14. A.Z. Simões, M.A. Ramirez, C.S. Riccardi, E. Longo, J.A. Varela, Ferroelectric properties and leakage current characteristics of $Bi_{3.25}La_{0.75}Ti_3O_{12}$ thin films prepared by the polymeric precursor method. J. Appl. Phys. **98**(11), 114103-1–114103-5 (2005)

15. N.S.L.S. Vasconcelos, J.S. Vasconcelos, V. Bouquet, S.M. Zanetti, E.R. Leite, E. Longo, L.E.B. Soledade, F.M. Pontes, M. Guilloux-Viry, A. Perrin, M.I. Bernardi, J.A. Varela, Epitaxial growth of $LiNbO_3$ thin films in a microwave oven. Thin Solid Films **436**(2), 213–219 (2003)

16. B. Nagaraj, S. Aggarwal, R. Ramesh, Influence of contact electrodes on leakage characteristics in ferroelectric thin films. J. Appl. Phys. **90**(1), 375–382 (2001)

17. C.C. Yang, M.S. Chen, T.J. Hong, C.M. Wu, J.M. Wu, T.B. Wu, Preparation of (100)-oriented metallic $LaNiO_3$ thin films on Si substrates by radio frequency magnetron sputtering for the growth of textured $Pb(Zr_{0.53}Ti_{0.47})O_3$. Appl. Phys. Lett. **66**(20), 2643–2645 (1995)

18. M.S. Chen, T.B. Wu, J.M. Wu, Effect of textured $LaNiO_3$ electrode on the fatigue improvement of $Pb(Zr_{0.53}Ti_{0.47})O_3$ thin films. Appl. Phys. Lett. **68**(10), 1430–1432 (1996)

19. C.D. Ling, M. Johnson, Modelling, refinement and analysis of the 'Type III' δ-Bi_2O_3-related superstructure in the Bi_2O_3–Nb_2O_5 system. J. Solid State Chem. **177**(6), 1838–1846 (2004)

20. J. Lu, S. Stemmer, Low-loss, tunable bismuth zinc niobate films deposited by rf magnetron sputtering. Appl. Phys. Lett. **83**(12), 2411–2413 (2003)

21. R. Miida, M. Tanaka, A modulated structure in a fluorite-type fast-ion-conductor δ-(Bi_2O_3) $(Nb_2O_5)_x$. Jpn. J. Appl. Phys. **29**(6R), 1132–1138 (1990)

22. A. Gulino, S. La Delfa, I. Fragalà, R.G. Egdell, Low-temperature stabilization of tetragonal zirconia by bismuth. Chem. Mater. **8**(6), 1287–1291 (1996)

23. M. Valant, B. Jancar, U. Pirnat, D. Suvorov, The order–disorder transition in Bi_2O_3–Nb_2O_5 fluorite-like dielectrics. J. Eur. Ceram. Soc. **25**(12), 2829–2834 (2005)

24. K. Tabata, T. Choso, Y. Nagasawa, The topmost structure of annealed single crystal of $LiNbO_3$. Surf. Sci. **408**(1), 137–145 (1998)

25. V.V. Atuchin, I.E. Kalabin, V.G. Kesler, N.V. Pervukhina, Nb 3d and O 1 s core levels and chemical bonding in niobates. J. Electron Spectrosc. Relat. Phenom. **142**(2), 129–134 (2005)

26. J.M. Carlsson, B. Hellsing, H.S. Domingos, P.D. Bristowe, Theoretical investigation of the pure and Zn-doped alpha and delta phases of Bi_2O_3. Phys. Rev. B. **65**(20), 205122–205132 (2002)

27. H.W. Lee, W.J. Lee, S.G. Yoon, Dielectric Bi_3NbO_7 thin films deposited on polymer substrates by nanocluster deposition for flexible electronic device applications. Electrochem. Solid-State Lett. **12**(5), G23–G26 (2009)

28. G. Dietz, M.R. Schumacher, R. Waser, S.K. Streiffer, C. Basceri, A.I. Kingon, Leakage currents in $Ba_{0.7}Sr_{0.3}TiO_3$ thin films for ultrahigh-density dynamic random access memories. J. Appl. Phys. **82**(5), 2359–2364 (1997)

29. J.F. Scott, Device physics of ferroelectric thin-film memories. Jpn. J. Appl. Phys. 1 **38**(4), 2272–2274 (1999)

30. A.Q. Jiang, Z.X. Hu, L.D. Zhang, The induced phase transformation and oxygen vacancy relaxation in La-modified bismuth titanate ceramics. Appl. Phys. Lett. **74**, 114–116 (1999)

31. J. Zhai, H. Chen, Ferroelectric properties of $Bi_{3.25}La_{0.75}Ti_3O_{12}$ thin films grown on the highly oriented $LaNiO_3$ buffered Pt/Ti/SiO_2/Si substrates. Appl. Phys. Lett. **82**(3), 442–444 (2003)

32. H.J. Cho, W. Jo, T.W. Noh, Leakage current behaviors in rapid thermal annealed $Bi_4Ti_3O_{12}$ thin films. Appl. Phys. Lett. **65**(12), 1525–1527 (1994)

33. A.I. Kingon, S. Srinivasan, Lead zirconate titanate thin films directly on dielectric and piezoelectric applications. Nat. Mater. **4**(3), 233–237 (2005)